HHS Public Access

Author manuscript

Magn Reson Imaging. Author manuscript; available in PMC 2015 October 24.

Published in final edited form as:

Magn Reson Imaging. 2014 July ; 32(6): 693–701. doi:10.1016/j.mri.2014.03.007.

Wireless MR Tracking of Interventional Devices Using Phase-Field Dithering and Projection Reconstruction

Martin A. Rube[1], **Andrew B. Holbrook**[2], **Benjamin F. Cox**[1], **J. Graeme Houston**[3], and **Andreas Melzer**[1]

[1]Institute for Medical Science and Technology, Division of Imaging and Technology, University of Dundee, Dundee, United Kingdom

[2]Department of Radiology, Stanford University, Stanford, California, United States

[3]Department of Clinical Radiology, Ninewells Hospital and Medical School, NHS Tayside, Dundee, UK

Abstract

Purpose—Device tracking is crucial for interventional MRI (iMRI) because conventional device materials do not contribute to the MR signal, may cause susceptibility artifacts and are generally invisible if moved out of the scan plane. A robust method for wireless tracking and dynamic guidance of interventional devices equipped with wirelessly connected resonant circuits (wRC) is presented.

Methods—The proposed method uses weak spatially-selective excitation pulses with very low flip angle (0.3°), a Hadamard multiplexed tracking scheme and employs phase-field dithering to obtain the 3D position of a wRC. RF induced heating experiments (ASTM protocol) and balloon angioplasties of the iliac artery were conducted in a perfused vascular phantom and three Thiel soft-embalmed human cadavers.

Results—Device tip tracking was interleaved with various user-selectable fast pulse sequences receiving a geometry update from the tracking kernel in less than 30 ms. Integrating phase-field dithering significantly improved our tracking robustness for catheters with small diameters (4–6 French). The volume root mean square distance error was 2.81 mm (standard deviation: 1.31 mm). No significant RF induced heating (<0.6°C) was detected during heating experiments.

Conclusion—This tip tracking approach provides flexible, fast and robust feedback loop, intuitive iMRI scanner interaction, does not constrain the physician and delivers very low specific absorption rates. Devices with wRC can be exchanged during a procedure without modifications to the iMRI setup or the pulse sequence. A drawback of our current implementation is that position information is available for a single tracking coil only. This was satisfactory for balloon angioplasties of the iliac artery but further studies are required for complex navigation and catheter shapes before animal trials and clinical application.

Corresponding author and reprint information: Martin Rube, Institute for Medical Science and Technology, University of Dundee, Wilson House, 1 Wurzburg Loan DD2 1FD, Dundee, United Kingdom, Fax: +44 (0) 1382 3 86588; Tel: +44 (0) 1382 3 88593; martin.a.rube@gmail.com.

Introduction

Magnetic Resonance Imaging (MRI) is an appealing modality for guiding cardiovascular interventions as it provides contrast between normal and abnormal soft tissues more precisely than any other imaging modality (1). MRI also allows for multi-planar imaging capability without ionizing radiation exposure or need for iodine based contrast agents.

Despite the number of advantages, MRI is not widely accepted as an interventional imaging modality with the majority of procedures being performed predominately at academic health centers (2). Interventional MRI (iMRI) and iMRI workflow is greatly influenced by the limited patient access and the requirement to ensure MRI safety throughout a procedure (3). During iMRI, operator/physician interaction is required for acquiring and displaying images according to the position and orientation of the interventional device. This is particularly important for endovascular procedures, where blood flow and respiratory motion are present during device manipulation. Interactions with the MRI system, in terms of device localization and change of acquisition parameters, are challenging (4) in comparison to conventional X-Ray guided procedures and represent a major hurdle for an efficient workflow (2, 5).

Safe, reliable, and easy to use tracking and visualization of moving devices are therefore key elements for successful clinical implementation of iMRI (6). Over the past decades, several device visualization and tracking methods have been developed for iMRI, using either passive susceptibility markers (7, 8), a wirelessly connected resonant circuit (9) (wRC), or active micro receive coils (10) that require a physical (wire based) connection to the MR scanner.

This manuscript describes a modified application of MR-tracking, based on the method introduced by Dumoulin and colleagues (10). Dumoulin's method requires at least one micro receive coil attached to an interventional device, which is connected to a receiver channel of the MRI scanner (10). The location of each micro coil in space is computed with a dedicated tracking pulse sequence that employs one-dimensional (1D) projection readouts (10). This method was dramatically improved in Dumoulin's publication in 2010 (11) in which phase-dithering was added at the expense of increased scanning time. Phase-dithering employs modulated dephasing magnetic field gradient pulses orthogonally to each 1D projection readout (11). Phase-dithering removes issues encountered when working with situations where signal dephasing occurs due to pulsatile flow, issues resulting from the proximity of imaging coils (i.e. B_1 effects or coupling of the microcoils with the body or surface coils (11)), as well as due to complex susceptibility artifacts.

MR-tracking using phase-dithering was applied to wRC that inductively couple to the surface receiver coils of an MRI system. Device tracking based on wRCs presents a promising solution for iMRI because no electrically conductive connection between the device tip and the MRI scanner is required. This avoids the risk of radiofrequency (RF) induced tissue heating (12–14) and reduces system complexity in terms of engineering and procedure workflow.

This MR tip tracking sequence was also interleaved with various fast, user-selectable pulse sequences that generated different contrast mechanisms with potentially different temporal resolutions. Each imaging sequence received a frequent geometry update from the tracking kernel. The coil position was also mapped to a pre-acquired 3D angiographic roadmap.

This work serves as a feasibility study of wireless device tracking to be used during iMRI and was demonstrated on a clinical 1.5 T MRI scanner by means of arterial flow phantom and Thiel soft-embalmed human cadaver (15–17) experiments.

Methods

Device Design

wRCs are based on the principle of electromagnetic induction, where an electric circuit is tuned to resonate at the proton Larmor frequency f_0 of the imaging system (9). A high quality factor of the wRC results in a significant amplification in central flux and even RF pulses with low FA can result in a substantial rotation of magnetization within the coil (9). The background, on the contrary, gives relatively little signal compared to the amplified signal (18).

It has been proposed (9, 19) to use a small object containing a solution with very short T_1 within the coil of the wRC to enhance this effect. However, this is not applicable for our purposes, as endovascular procedures are performed according to Seldinger (20), whereby catheters are placed over a guidewire, and essentially no MR signal-carrying lumen can be used to contribute to the signal amplification.

The coil of the wRC was designed as a planar rectangular spiral coil (Figure 2), made of enameled copper-wire (0.2 mm, 2UEWF, Conrad, Hirschau, Germany), and connected to a non-magnetic SMD-capacitor (VJ0402, Vishay, Malvern, PA, US). The wRC (Figure 2) was tuned in 0,9% saline solution to f_0= 63.8 MHz, the proton Larmor frequency at 1.5 T, using a spectrum analyzer (HMS1000, HAMEG, Mainhausen, Germany). A wRC was attached to the tip of a commercially available non-braided 5-French (F) catheter (Royal Flush, Straight, Cook, Bloomington, IN, US) and a 5-F balloon catheter (Advance 35LP, Cook, Bloomington, IN, US) with medical grade heat shrink tubing (Advanced Polymers, Salem, NH, US). We measured a quality factor of approximately 65 in 0.9% saline solution.

RF induced heating was evaluated according to the ASTM protocol (ASTM F2182-09), originally developed for RF induced heating on or near passive implants during MRI (21). The temperature was recorded with gallium arsenide temperature sensors connected to a measurement unit (Fotemp4, Optocon AG, Dresden, Germany) via optical fibers. The measurement unit was positioned outside of the Faraday cage and the optical fibers were fed through the wave-guides. Three temperature probes were attached (distal, medial, proximal) to the wRC and one probe to the patient table as reference. The wRC was then positioned in a head-torso phantom filled with a tissue equivalent gel (21) (water, 1.32 g/L NaCl, 10 g/L polyacrylic acid partial sodium salt (Sigma-Aldrich Corp., Saint Louis, Missouri, USA)). Fast spin echo (21) imaging (TE/TR = 14/425 ms, ETL = 4, FOV = 40 cm × 40 cm, Matrix = 256 × 256, Slice thickness = 10 mm) was performed in a 1.5 T MRI scanner (Signa HDx,

Software Release 15.0_M4A, GE Healthcare, Waukesha, WI, USA) with the integrated body coil (transmit/receive). This sequence was prescribed for approximately 15 minutes and produced an averaged whole body specific absorption rate (SAR) of 2 W/kg.

Tracking Pulse Sequence

Weiss et al. (22) suggested using low FA RF excitation pulses and projection readouts to localize a wRC during iMRI. We adopted and integrated this concept into a dedicated non-imaging MR pulse sequence proposed by Dumoulin and colleagues (11). Unlike this active tracking pulse sequence, our tracking sequence employed non-spatially-selective or weakly-spatially-selective RF excitation pulses with very low FA and also spoiling gradients at the end of each repetition to dephase the magnetization, and thus (for low FA excitations) reduce phase coherences.

The pulse sequence diagram is shown in Figure 1. The Hadamard readout (HR) scheme provided three dimensions of positional information within four excitations. Therefore, our implementation required four times the number of different dephasing gradient directions (N × 4 × TR) to compute the most accurate position of the wRC.

Ideally the coil of the wRC should have had all dimensions matching the readout resolution. This would have resulted in a very sharp peak in the presence of magnetic field gradients and hence spatially very accurate tracking results. However, for our (non-ideal) wRC design (Figure 2) it was essential to use the center of mass for the peak detection algorithm and not the maximum signal intensity value, as the broad peak represents a relatively large area of spins with amplified FA in close vicinity of the wRC.

The tracking sequence was implemented with standard multiple receiver imaging coils and no limitation of receiver channels. Therefore, the peak-to-noise ratio (PNR) was taken into account for each coil element. The coil element with the highest PNR (for a given phase-dithering direction) was selected as this represents the coil element that inductively couples best to the wRC. The catheter tip position was then computed in the MRI coordinate system after a gradient warp correction for gradient nonlinearities.

The tracking pulse sequence parameters were used as follows: Time of Echo (TE) = 1.52 ms, Time of Repetition (TR) = 2.18 ms, FA = 0.3°, FOV = 48 cm along the readout direction, Isotropic tracking resolution = 1.8 mm, Slice thickness = 300 mm.

Imaging Pulse Sequence

The tracking sequence was interleaved with one or more user-selectable rapid imaging sequences in a closed loop manner. This is illustrated in Figure 2c. The position of the tip of the interventional device was detected by the tracking sequence and then used to automatically adjust the scan plane of the following imaging slice. Spoiling gradients were applied at the end of the imaging sequence to dephase the magnetization, and thus (for low flip angles) reduce phase coherences before a subsequent low FA excitation was employed in the tracking sequence.

Three different imaging sequences were implemented that received a scan plane update from the tracking sequence. First, a balanced steady-state free precession (bSSFP) sequence using a Cartesian k-space data acquisition scheme and generating T_2/T_1 contrast (23, 24) was realized. Second, a fast spoiled gradient recalled echo (FSPGR) sequence with Cartesian k-space acquisition scheme generating high spatial resolution and T_1 contrast (25) was integrated. Third, a gradient recalled echo (GRE) sequence with spiral k-space data acquisition scheme (spGRE) was designed to achieve a high temporal resolution. The operator was able to select each imaging sequence through the control console on the fly.

Figure 1c illustrates how each imaging sequence received a coordinate and geometry update and was executed after a steady state stabilization interval. As previously proposed (26), a non linear ramp-up with eight consecutive RF pulses ($\beta = 3$) was used to transfer the initial longitudinal magnetization toward its steady state prior to bSSFP data acquisition. Alternatively, a stabilization interval employing 40 dummy repetitions (27) was used prior to FSPGR data acquisition.

The imaging parameters for the bSSFP were as follows: TE/TR = 2.5/5.0 ms, FA = 70°, FOV = 30 cm × 30 cm, Matrix 256×256, Slice thickness = 5 mm. The imaging parameters for the FSPGR were as follows: TE/TR = 2.8/5.6 ms, FA = 30°, FOV = 30 cm × 30 cm, Matrix 256×256, Slice thickness = 5 mm. Five 10.65 ms spiral readouts were used to cover k-space for an FOV of 24 cm to achieve an in-plane resolution of 0.9 mm and a temporal resolution of 10 frames per second (fps) for the spGRE.

The catheter tip position was also used in a previously acquired static 3D MR angiography (MRA) road map for catheter guidance. As proof of principle a bright blood SPGR time of flight (ToF) (28) sequence was integrated into the iMRI interface producing a 2D stack of non-contrast enhanced MRA (nonCE-MRA) images. The 2D SPGR TOF sequences was used with a TE/TR = 2.3/18.0 ms, FA = 30°, FOV = 20 cm × 20 cm, Matrix = 256×256, Slice thickness = 2 mm with 20% gap between slices.

Real-Time MRI Implementation

All iMRI experiments were performed in a clinical 1.5 T MRI scanner (Signa HDx, Software Release 15.0_M4A, GE Healthcare, Waukesha, WI, USA) with a novel interventional coil consisting of a single loop (posterior) and a 4-channel paddle element (anterior) (DuoFlex, MR Instruments, Minnetonka, MN, USA).

Two-way data communication between the MRI scanner and an external high performance Linux (Ubuntu 12.04 64bit) workstation (16-CPU, 32 GB memory, z820, Hewlett-Packard, Palo Alto, CA) was accomplished via Gigabit Ethernet. The pulse sequences were designed in a graphical pulse sequence environment (SpinBench, Version 1.3.2, HeartVista, Inc., Palo Alto, CA, USA) and implemented in RTHawk (29) (RTHawk, Version 0.9.28, HeartVista, Inc., Palo Alto, CA, USA), running on the external workstation.

A real-time visualization application (30) (Vurtigo, Version 2-1b, Sunnybrook Health Sciences Centre, Toronto, Canada) embedded in RTHawk, was used to render the tip position, the current scan plane, and optionally a 3D MRA dataset. This allowed the user to

view the real-time catheter tip position connected to the rt-MRI scan plane and also to monitor the catheter movement overlaid to a maximum intensity projection (MIP) of the nonCE-MRA dataset. The performance of the tracking kernel for reliable detection of the catheter was optimized and evaluated by moving the straight catheter through the imaging volume along known reference points.

Phantom Experiments

Phantom experiments (20 repetitions) were conducted by two experienced interventional radiologists in an arterial vessel phantom consisting of an above the knee lower extremities (LE), an abdominal and a thoracic module (Elastrat, Sarl, Switzerland). The phantom was connected to a modified heart lung machine (HL-30, Maquet, Rastatt, Germany) and perfused with 0.9% saline solution to mimic the electrical and relaxation properties of blood (T_1 ~ 1150 ms, T_2 ~ 130 ms at 1.5 T and 20 °C). The pump was positioned outside the scan room and set to a flow rate of 4.8 L/min, a heart rate of 85 beats per minute and a systolic/diastolic pressure of approximately 130 / 70 mmHg. The containers of the vessel phantom were backfilled with a 10% gelatinous solution to mimic muscle tissue (T_1 ~ 846 ms, T_2 ~ 51 ms at 1.5 T and 20 °C). Vascular access was established with a 12-F introducer sheath (Check-Flo, Cook Inc., Bloomington, IN, US) on the right femoral LE. All catheters were inserted over a novel 0.035” MRI safe polymer guidewire (35) (MRLine, EPFlex, Dettingen/Erms, Germany) that was developed in collaboration with EPFlex and has recently received CE mark. The balloon catheter was inflated with a 1:100 Gd-DOTA (Dotarem; Guerbet, RoissyCDG Cedex, France) doped solution to allow positioning verification and to monitor the dilatation process.

Thiel soft embalmed human cadaver experiments

The human cadavers used in this study were donated according to standard procedures as set out in the Human Tissue (Scotland) Anatomy Act 2006, and the Thiel Advisory Committee (University of Dundee, UK) has approved all procedures involving human cadavers. The cadavers were embalmed according to the Thiel soft-fix embalming method as currently in use in our group (17). Thiel embalmed cadavers have been further developed in Dundee as a model for iMRI research and training with re-established respiratory motion (32) and partial reperfusion (33) and our group recently published the feasibility of MRI of Thiel soft-embalmed cadavers (16).

Three different cadavers (2 male and 1 female, age range 50 – 70, weight 65 – 80 kg) were prepared in the angio-suite (OEC 9900 Elite, GE Medical Systems, Waukesha, WI, USA) and then each cadaver was transferred to the MRI for the experiments (MR surgical suite, GE Medical Systems and Maquet, Rastatt, Germany). Vascular access was established with a 12-F introducer sheath (Check-Flo, Cook Inc., Bloomington, IN, US) in the left femoral artery. The femoral artery was then flushed with 0.9% saline solution to mimic the electrical properties of blood.

Two experienced interventional radiologists evaluated the proposed methods by navigating the straight catheter over the MR-safe guidewire in the femoral artery. No 3D roadmap was

acquired for the cadaver experiments due to the absence of perfusion (extravasation and no venous return).

Results

All catheters with wRCs remained functional throughout the flow phantom and cadaver experiments. The wRCs resulted in an increase in mechanical stiffness and an outer diameter of 2.4 mm (7-F) of both catheters. This prohibited their use in vessels with an inner diameter of 3 mm or less. The maximum temperature (measured at three locations of the resonant marker) did not exceed 0.6 °C over the entire duration of the RF induced temperature measurement, which was performed according to the ASTM protocol (21).

Phantom Experiments

Figure 4 illustrates the signal after FFT for four different receive coil channels. Each coil element was receiving MR signals during a tracking cycle with phase-field dithering (N=3) while the 5-F straight catheter was navigated through the phantom. The coil element with the highest PNR averaged over the 4 HR is plotted in Figure 5 (same phase field dithering cycle as in Figure 4), which was automatically selected by the peak detection algorithm. Without phase-field dithering, catheter positions were not adequately resolved due to high background noise.

An area with enhanced FA was clearly visible at the tip of the catheter, once the wRC was located in the imaging slice, after a coordinate update (Figure 7b). The tracking kernel provided up to 38 catheter position updates per second. The tracking sequence delivered very low SAR compared to standard imaging pulse sequences because of the low FA excitation.

Distance errors were measured as the difference between the tracking position and the center of gravity the catheter tip (Xc,Yc,Zc) as displayed in Figure 6a. The center of gravity is depicted as sphere in Figure 6a. The tracking accuracy was dependent on the position and angulation of the wRC relative to each of the surface coil elements. All tracking points were found to be inside the area of enhanced signal resulting from the wRC on the catheter tip. The statistical summary for the distance error is displayed in (Figure 6b). The volume root mean square (RMS) distance error was 2.81 mm, the mean distance error in 3D was 2.49 mm and the standard deviation was 1.31 mm.

The imaging pulse sequences received a frequent geometry update (26 ms were required to execute the tracking pulse sequence and to compute and update the position information) from the tracking kernel and the coil position was also mapped to a pre-acquired 3D roadmap. Figure 7 illustrates the ability to switch between different sequences during a procedure with each sequence tailored to the particular task at hand. The tracking position was stable while navigating through the femoral artery, iliac artery and the aorta. The position remained adequate during balloon inflation in the right iliac artery (Figure 7c). The operator was able to switch back and forth between different pulse sequences (one mouse click, no time delay) while each sequence was receiving an adequate coordinate update.

A 2D spGRE plane was fused to a 3D nonCE-MRA roadmap Figure 8a. Then a catheter was inserted and advanced while the imaging plane was continuously re-aligned to the updated tracking position of the catheter (Figure 8b). A 2D view of a FSPGR sequence while the slice was updated to the current catheter position (sphere) is demonstrated in Figure 8c. The catheter position was also mapped to the roadmap (Figure 8b) according to the preference of the physician and was optionally used to realign the scan plane to the current catheter position (Figures 8d–f).

Thiel soft embalmed human cadaver experiments

During our experiments, two interventional radiologists successfully inserted and navigated the straight catheter (5-F) through the femoral artery of three Thiel soft embalmed cadavers. Figure 9 illustrates the signal after FFT for four different receive coil channels similar to what was described for the phantom experiments. Each coil element was receiving MR-tracking signals during a tracking cycle with phase-field dithering (N=3). The PNR was calculated for each HR and is displayed in Figure 9 above each peak. During catheter navigation and continuous movement the PNR was found to exceed a value of 10 along all readout directions (data not shown). The sequence parameters required optimization for the Thiel embalmed human cadaver. Hence, a FA of 1.5° and smoothing of the curve were applied to improve the PNR.

During catheter navigation an area with enhanced FA was clearly visible (Figure 10) at the tip of the catheter after a coordinate update was received and executed. The Figure 10 illustrates interactive switching between different pulse sequences during the catheterization of the femoral artery of a Thiel soft embalmed cadaver. This was enabled on request of the operating physician, depending on his preference of high spatial or temporal resolution. Figure 10e illustrates the tracking positions that were found for 1000 repetitions of the tracking pulse sequence with phase-field dithering (N=3) while the catheter was maintained in the same position.

Discussion

A wireless tracking sequence employing phase-field dithering and projection reconstruction was developed and interleaved with various user-selectable fast pulse sequences to facilitate cardiovascular interventions in clinical whole body MRI scanners. The proposed methods do not require hardware modifications of the MRI scanner setup and address the key issue of robust MR tracking.

On the other hand, active tracking based on physically connected micro coils mounted at catheter distal ends has widely been used (4, 10, 11, 34, 35) and provides an excellent, reliable and very robust form of MR tracking. However, these micro receive coils of the catheter have to be connected to the MRI system in a similar fashion as imaging coils. This constitutes a significant technical hurdle, potential cable loops (36) and increased cost of producing these catheters.

Standing waves along conducting cables that approach the quarter wavelength of the RF excitation field are the primary source of instrument heating in the MRI environment. This

can still be a potential safety hazard for active tracking (4, 18) and temperature rises of more than 50 °C and sparks (14) have been reported for long conductive structures (13, 37). The regulatory hurdles in this context are significant because safety throughout the procedure has to be guaranteed.

Various methods such as quarter-wavelength coaxial chokes (38) or integration of transformers into the transmission line (39) have been proposed to eliminate resonant RF heating in active tracking catheters. These have shown to overcome the heating risks but would further increase challenges for the design and production of these, mainly single use, catheters. Hence, widespread use of active tracking in humans during iMRI is still limited due to the system complexity and design challenges (8) to overcome safety hazards and achieve the mechanical properties (i.e. torque transmission and elasticity) for the used clinical devices. Active tracking, however, provides an accurate and reliable solution for clinical applications where the patient and cable connections do not come in contact e.g. for real-time position tracking of a transducer during MRI-guided focused ultrasound surgery (40).

This tracking implementation is based on small resonant circuits that wirelessly couple to the MRI transmit and receive coils (9) and does not utilize long electrical conductors (18). No significant heating (<0.6°C) was detected during the RF induced heating experiments according to the ASTM protocol (21).

Phase-field dithering, similar as described by Dumoulin et al. for active tracking (111), has significantly improved the tracking accuracy and the peaks in the MR tracking were adequately resolved. The accuracy of the proposed tracking method was found to be similar to methods that were proposed for active catheter tracking and cited an overall accuracy in the range of +/− 2–4 mm (34, 41). Similarly, the time that was required for a positional update was approximately 26 ms, which is comparable to active tracking methods ranging between 20 ms (11) and 24 ms (4). Further improvement for this tracking pulse sequence is possible by averaging over multiple tracking cycles, at the expense of increased scanning time.

The results of the phantom and cadaver experiments successfully demonstrate that fast and reliable detection of wRCs is feasible and may successfully be employed for iMRI applications. The PNR of the cadaver experiments was lower compared (Figure 9) to the idealized phantom experiments (Figure 5). However, MR imaging of Thiel soft-embalmed cadavers is constrained (16) and constitutes the worst case as living organisms provide better RF penetration (16) and it is foreseen that imaging and tracking will improve in animal and patient studies.

Additionally, it would be desirable for complex catheter shapes and challenging vascular navigation to obtain more than one tracking position on catheters to determine the tip orientation in particular where the tip can fold on itself (i.e. create a loop of the shaft near the tip), which cannot be detected with a single coil. Therefore it was proposed to use multiple independent micro receive coils for active catheter tracking (4, 10, 30). In our implementation, if more than one wRC is used, multiple signals would couple to the receive

coils resulting in multiple peaks per projection readout. These peaks would correspond to a range of possible 3D position candidates after computation of the Hadamard encoded readouts. To overcome this problem, an algorithm for fast 3D localization of several wRCs has been proposed (19) and applied in prostate biopsies (using 3 wRCs containing a MR signal-carrying lumen each). This method (19) could potentially also be adapted for MR tracking of multiple wRCs on catheters employing phase-field dithering, which has to be investigated in further studies.

Another interesting approach to address this problem has recently been proposed by combining a single wRC on the tip of the catheter and passive susceptibility markers along the shaft (42). This catheter could also be used with our tracking implementation (no modifications required) while the wRC on the tip is used for tip tracking (and scan plane updates) and the passive markers for catheter shaft visualization.

Our implementations offer reliable catheter tip localization and scan position updates in combination with the ability to switch between high- and low-resolution as well as different contrast mechanisms. Despite the fact that the results with bSSFP or FSPGR imaging were obtained with approximately one fps, higher frame rates could easily be achieved by utilizing parallel imaging (43, 44) or other acceleration techniques while not affecting the tracking robustness. The presented spGRE achieved frame rates up to 10 fps and was found useful for imaging of dynamic processes e.g. for blood flow proximal and distal to an occluded vessel pre and post treatment. Higher frame rates utilizing spGRE may be possible; however this would compromise image quality.

All MRI controls were embedded in a dedicated user interface that was optimized for cardiovascular interventions within the RTHawk real-time framework (29). While the 2D display was the preferred guidance method, our interventional radiologists rated the real-time tip tracking position displayed in the 3D roadmap very useful, particularly during the initial steps of an intervention. This was also preferred when exact positioning under rt-MRI guidance was not essential or in anatomical structures with complex vasculature that could not be imaged within a single 2D plane. The tracking position displayed in the roadmap can also be particularly useful when low SAR exposure is a key requirement.

In this study, two different (straight/balloon) catheters were prepared with wRCs to demonstrate fast sequence interchange ability during a procedure. All catheters for this study were in house prototyped. However, a major hurdle to clinical evaluation is the integration of wRCs with a sufficient quality factor into the catheter design (38). Ideally, the coil design (Figure 2) should have had all dimensions matching the readout resolution but with current manufacturing technologies, we were not able to achieve a sufficient Q for the given catheter dimensions. Alternatively, a higher Q could have been achieved by increasing the diameter of the copper wire. However, this was discarded because a larger outer diameter would necessitate arterial access of a larger caliber and limits the use to interventions in larger vessels only. The stiffness and increased outer diameter is a temporary problem of manually wound wRCs and recently micro systems based technologies for production of wRCs have been validated (45, 46). In the future, these optimized and miniaturized wRCs, will enhance the tracking accuracy and alleviate negative catheter changes (e.g. increased

diameter, stiffness and glide). However, these manufacturing technologies have to be evaluated to understand if sufficient quality factors can be achieved.

In conclusion, we have presented a feasible concept for fast and robust wireless device tracking that is not limited to catheters and can in principle be used on any device (e.g. a guidewire or needle) with a wRC. The wireless tracking can be combined with various pulse sequences and does not require any changes to the MR scanner hardware. Our implementation reduces complexity, minimizes user interaction with the MRI system and provides the interventional radiologist with a flexible and intuitive tool to perform cardiovascular interventions under rt-MRI guidance.

Acknowledgments

We thank Juan Santos, Joelle Barral and William Overall for helpful input and discussions. Also, we thank Leonard Fass and John Ferrut as well as Tom Breslin and Gabor Mizsei for their friendly and helpful support. We are in particular grateful for the help and input from Labonny Biswas. The authors also acknowledge the funding sources NIH R01-CA121163 and P01-CA159992. The authors are thankful for financial assistance provided by the FUSIMO ("Patient specific modeling and simulation of focused ultrasound in moving organs") project funded under the European Community's Seventh Framework Programme (FP7/2007–2013) for Research and Technological Development under Grant Agreement no 270186. The Marie Curie Initial Training Network supported this work and the Integrated Interventional Imaging Operating System (IIIOS) project has received funding from the European Community's Seventh Framework Programme (FP7/2007–2013) under Grant Agreement no 238802.

References

1. Gedroyc WM. Interventional magnetic resonance imaging. BJU INT. 2000; 86(1):174–180. [PubMed: 10961287]
2. Rothgang E, Gilson WD, Wacker F, Hornegger J, Lorenz CH, Weiss CR. Rapid freehand MR-guided percutaneous needle interventions: An image-based approach to improve workflow and feasibility. J Magn Reson Imaging. 2013; 37(5):1202–1212. [PubMed: 23334924]
3. Jolesz, Fa; Nabavi, A.; Kikinis, R. Integration of interventional MRI with computer-assisted surgery. J Magn Reson Imaging. 2001; 13(1):69–77. [PubMed: 11169806]
4. Bock M, Volz S, Zühlsdorff S, Umathum R, Fink C, Hallscheidt P, Semmler W. MR-guided intravascular procedures: real-time parameter control and automated slice positioning with active tracking coils. J Magn Reson Imaging. 2004; 19(5):580–589. [PubMed: 15112307]
5. Fernández-Gutiérrez F, Barnett I, Taylor B, Houston G, Melzer A. Framework for detailed workflow analysis and modelling for simulation of multi-modal image-guided interventions. J Enterprise Inform Manag. 2013; 26(1):75–90.
6. Melzer, A.; Immel, E.; Toomey, R.; Fernandez-Gutierrez, F. MR-guided interventions and surgery. In: Kramme, R.; Hoffmann, K-P.; Pozos, RS., editors. Springer Handbook of Medical Technology. Springer Berlin Heidelberg; 2011. p. 477-501.
7. Bakker CJ, Hoogeveen RM, Weber J, van Vaals JJ, Viergever Ma, Mali WP. Visualization of dedicated catheters using fast scanning techniques with potential for MR-guided vascular interventions. Magn Reson Med. 1996; 36(6):816–820. [PubMed: 8946346]
8. Patil S, Bieri O, Jhooti P, Scheffler K. Automatic slice positioning (ASP) for passive real-time tracking of interventional devices using projection-reconstruction imaging with echo-dephasing (PRIDE). Magn Reson Med. 2009; 62(4):935–942. [PubMed: 19585605]
9. Burl M, Coutts Ga, Young IR. Tuned fiducial markers to identify body locations with minimal perturbation of tissue magnetization. Magn Reson Med. 1996; 36(3):491–493. [PubMed: 8875424]
10. Dumoulin CL, Souza SP, Darrow RD. Real-time position monitoring of invasive devices using magnetic resonance. Magn Reson Med. 1993; 29(3):411–415. [PubMed: 8450752]
11. Dumoulin CL, Mallozzi RP, Darrow RD, Schmidt EJ. Phase-field dithering for active catheter tracking. Magn Reson Med. 2010; 63(5):1398–1403. [PubMed: 20432311]

12. Nitz WR, Brinker G, Diehl D, Frese G. Specific absorption rate as a poor indicator of magnetic resonance-related implant heating. Invest Radiol. 2005; 40(12):773–776. [PubMed: 16304480]
13. Nitz WR, Oppelt A, Renz W, Manke C, Lenhart M, Link J. On the Heating of Linear Conductive Structures as Guide Wires and Catheters in Interventional MRI. J Magn Reson Imaging. 2001; 114:105–114. [PubMed: 11169811]
14. Buecker A. Safety of MRI-guided vascular interventions. Minim Invasive Ther Allied Technol. 2006; 15(2):65–70. [PubMed: 16754188]
15. Thiel W. Eine Arterienmasse zur Nachinjektion bei der Konservierung ganzer Leichen. [An arterial substance for subsequent injection during the preservation of the whole corpse]. Ann Anat. 1992; 174:197–200. [PubMed: 1503237]
16. Gueorguieva MJ, Yeo DTB, Eisma R, Melzer A. MRI of Thiel-Embalmed Human Cadavers. J Magn Reson Imaging. 2013 [Epub ahead of print].
17. Eisma R, Lamb C, Soames RW. From formalin to thiel embalming: What changes? One anatomy department's experiences. Clin Anat. 2013; 26(5):564–571. [PubMed: 23408386]
18. Quick HH, Zenge MO, Kuehl H, Kaiser G, Aker S, Massing S, Bosk S, Ladd ME. Interventional magnetic resonance angiography with no strings attached: wireless active catheter visualization. Magn Reson Med. 2005; 53(2):446–455. [PubMed: 15678524]
19. Brujic D, Galassi F, Rea M, Ristic M. A novel algorithm for fast 3D localisation of N fiducial markers from 1D projections. Intl. Soc. Mag. Reson. Med. 2012; 20:2946.
20. Seldinger SI. Catheter Replacement of the Needle in Percutaneous Arteriography: A new technique. Acta Radiologica [Old Series]. 1953; 39(5):368–376.
21. ASTM International. F2182–09: Standard Test Method for Measurement of Radio Frequency Induced Heating On or Near Passive Implants During Magnetic Resonance Imaging. 2010
22. Weiss, S.; Schaeffter, T.; Luedeke, KM.; Leussler, C.; Holz, D.; Nehrke, K.; Rasche, V.; Sinkus, R. Intl. Soc. Mag. Reson. Med. Vol. 7. Philadelphia, PA, USA: 1999. Catheter localization using a resonant fiducial marker during interactive MR fluoroscopy; p. 1954
23. Deimling, M.; Heid, O. Proc. Intl. Soc. Mag. Reson. Med. Vol. 2. San Francisco, CA, USA: 1994. Magnetization prepared true FISP imaging; p. 495
24. Oppelt A, Graumann R, Barfuß H, Fischer H, Hartl W, Schajor W. FISP: eine neue schnelle Pulssequenz für die Kernspintomographie. Electromedica. 1986; 54:15–18.
25. Haase A, Frahm J, Matthaei D, Hänike W, Merboldt KD. FLASH Imaging. Rapid NMR Imaging Using Low Flip-Angle Pulses. J Magn Reson. 1986; 67(2):258–266.
26. Le Roux P. Simplified model and stabilization of SSFP sequences. J Magn Reson. 2003; 163(1): 23–37. [PubMed: 12852904]
27. Busse RF, Riederer SJ. Steady-state preparation for spoiled gradient echo imaging. Magn Reson Med. 2001; 45(4):653–661. [PubMed: 11283994]
28. Nishimura DG. Time-of-flight MR angiography. Magn Reson Med. 1990; 14(2):194–201. [PubMed: 2345502]
29. Santos, JM.; Wright, Ga; Pauly, JM. Conf Proc IEEE Eng Med Biol Soc. Vol. 2. San Francisco, CA, USA: 2004. Flexible real-time magnetic resonance imaging framework; p. 1048-1051.
30. Radau, PE.; Pintilie, S.; Flor, R.; Biswas, L.; Oduneye, SO.; Ramanan, V.; Anderson, KA.; Wright, GA. VURTIGO : Visualization platform for teal-time, MRI-guided cardiac electroanatomic mapping. In: Camara, O.; Konukoglu, E.; Pop, M.; Rhode, K.; Sermesant, M.; Young, A., editors. STACOM. Toronto, Canada: Springer-Verlag, Berlin Heidelberg; 2011. p. 244-253.
31. Rube, MA.; Seifert, P.; Bernhard, U.; Kakchingtabam, D.; Andre, P.; Melzer, A. Intl. Soc. Mag. Reson. Med. Vol. 20. Melbourne: 2012. Novel MR-safe guidewire with passive Iron-Platinum alloy nanoparticles for MR-guided interventions; p. 4239
32. Eisma R, Gueorguieva M, Immel E, Toomey R, McLeod G, Soames R, Melzer A. Liver displacement during ventilation in Thiel embalmed human cadavers - a possible model for research and training in minimally invasive therapies. Minim Invasive Ther Allied Technol. 2013 [Epub ahead of print].
33. Cox, BF.; Eisma, R.; Rube, MA.; Gueorguieva, M.; McLeod, H.; Immel, E.; Melzer, A. Developing Thiel Soft-Fix Cadavers as a suitable model for iMRI training and research. Proceedings of the 9th Inteventional MRI Symposium; Boston, MA, USA. 2012. p. 103

34. Wech, T.; Shea, SM.; Pan, L.; Barbot, J.; Vij, K.; Lorenz, CH.; Patil, S. Intl. Soc. Mag. Reson. Med. Vol. 19. Montreal, Quebec, Canada: 2011. Measurement Accuracy of Different Active Tracking Sequences for Interventional MRI; p. 1753Vol. 19.

35. Zimmermann H, Müller S, Gutmann B, Bardenheuer H, Melzer A, Umathum R, Nitz W, Semmler W, Bock M. Targeted-HASTE imaging with automated device tracking for MR-guided needle interventions in closed-bore MR systems. Magn Reson Med. 2006; 56(3):481–488. [PubMed: 16795081]

36. Dempsey MF, Condon B, Hadley DM. Investigation of the factors responsible for burns during MRI. J Magn Reson Imaging. 2001; 13(4):627–631. [PubMed: 11276109]

37. Konings MK, Bartels LW, Smits HF, Bakker CJ. Heating around intravascular guidewires by resonating RF waves. J Magn Reson Imaging. 2000; 12(1):79–85. [PubMed: 10931567]

38. Ladd ME, Quick HH. Reduction of resonant RF heating in intravascular catheters using coaxial chokes. Magn Reson Med. 2000; 43(4):615–619. [PubMed: 10748440]

39. Weiss S, Vernickel P, Schaeffter T, Schulz V, Gleich B. Transmission line for improved RF safety of interventional devices. Magn Reson Med. 2005; 54(1):182–189. [PubMed: 15968655]

40. Holbrook AB, Ghanouni P, Santos JM, Medan Y, Pauly KB. In vivo MR acoustic radiation force imaging in the porcine liver. Med Phys. 2011; 38(9):5081–5089. [PubMed: 21978053]

41. Hillenbrand CM, Elgort DR, Wong EY, Reykowski A, Wacker FK, Lewin JS, Duerk JL. Active device tracking and high-resolution intravascular MRI using a novel catheter-based, opposed-solenoid phased array coil. Magn Reson Med. 2004; 51(4):668–675. [PubMed: 15065238]

42. Rube, MA.; Immel, E.; Gandy, SJ.; Andre, P.; Samraj, P.; Houston, JG.; Melzer, A. Combined MRI visible Iron-Platinum (FePt) nanoparticles and a resonant tip marker for device localization and guidance in 1.5T and 3T MRI. Proceedings of the 97th Scientific Meeting of the Radiological Society of North America (RSNA); Chicago, Illinois, USA. 2011.

43. Pruessmann KP, Weiger M, Scheidegger MB, Boesiger P. SENSE: Sensitivity encoding for fast MRI. Magn Reson Med. 1999; 42:952–962. [PubMed: 10542355]

44. Sodickson DK, Manning WJ. Simultaneous acquisition of spatial harmonics (SMASH): Fast imaging with radiofrequency coil arrays. Magn Reson Med. 1997; 38(4):591–603. [PubMed: 9324327]

45. Detert M, Friesecke S, Deckert M, Rose G, Schmidt B, Kaiser M. Using the Hot Embossing Technology for the Realization of Microtechnical Structures in Medical Imaging. Biomed Tech. 2012; 57:599–602.

46. Kaiser, M.; Detert, M.; Schmidt, B.; Rose, G. Congress MedTech Pharma. Nuremberg, Germany: 2012. Technology Matrix: Production technologies of miniature instrument resonance markers for visualization under MRI.

47. Rube MA, Holbrook AB, Cox BF, Melzer L, Moritz L, Melzer A. Wireless remote control and in-room communication for MRIguided interventions using mobile touch devices. Int J CARS. 2013; 8(S1):5–11.

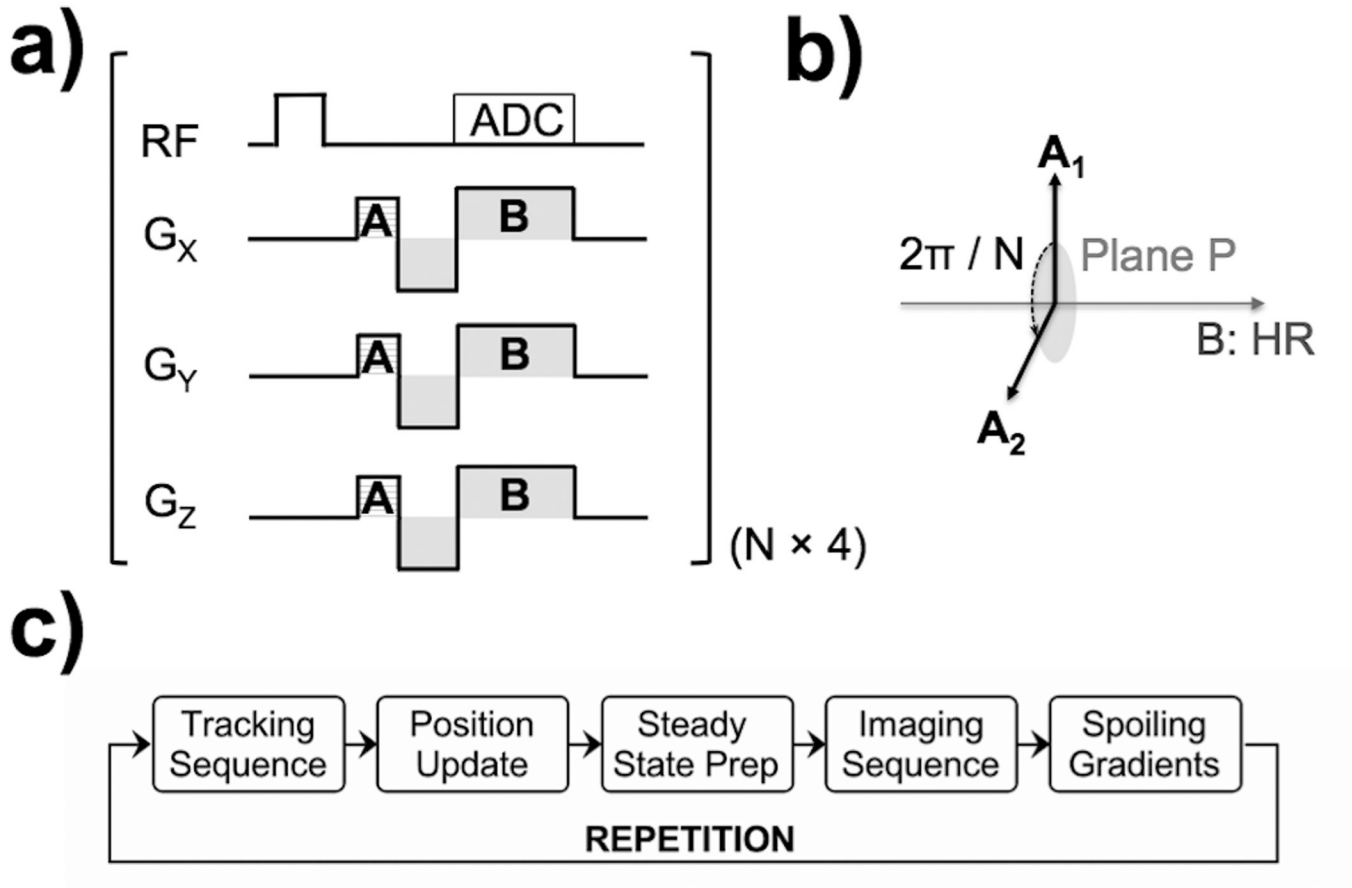

FIG. 1.

Pulse sequence diagram for detecting the position of the wRC – (a) A weakly selective RF excitation pulse with very low flip angle (FA) excites all spins within the active slab. The spins in the close vicinity of the wRC experience an amplified FA because a current is induced within the coil of the wRC. The frequency encoding gradient pulse (B) is multiplexed with a Hadamard scheme as described by Dumoulin et al. (10). Before the frequency encoding readout, phase-field dithering (A) is applied (11). The direction of the dephasing gradient (A) is chosen to be in a plane (P) perpendicular to the direction of the frequency encoding gradient pulse (B) as indicated in (b). An arbitrary choice is made for the first direction and the gradient direction is then rotated in the plane (P) by $2\pi/N$ for the next repetition. This tracking scheme requires N repetitions for the different dephasing directions multiplied by the four different Hadamard multiplexed frequency encoding gradient pulse directions. The polarity [Gx,Gy,Gz] of the gradient (B) for the four readouts is B1 = [+,+,+], B2 = [−,−,+], B3 = [−,+,−],B4 = [+,−,+]. The block diagram of the interleaved tracking and imaging pulse sequence with automated scan plane updates is demonstrated in (c). The wRC position is determined by the tracking kernel, which then automatically emits a coordinate update. The imaging sequence receives this new coordinate and geometry update and is executed after a steady state stabilisation interval. Finally, spoiling gradients are applied to dephase the magnetization, and thus (for low FA excitations) reduce phase coherences before the next repetition.

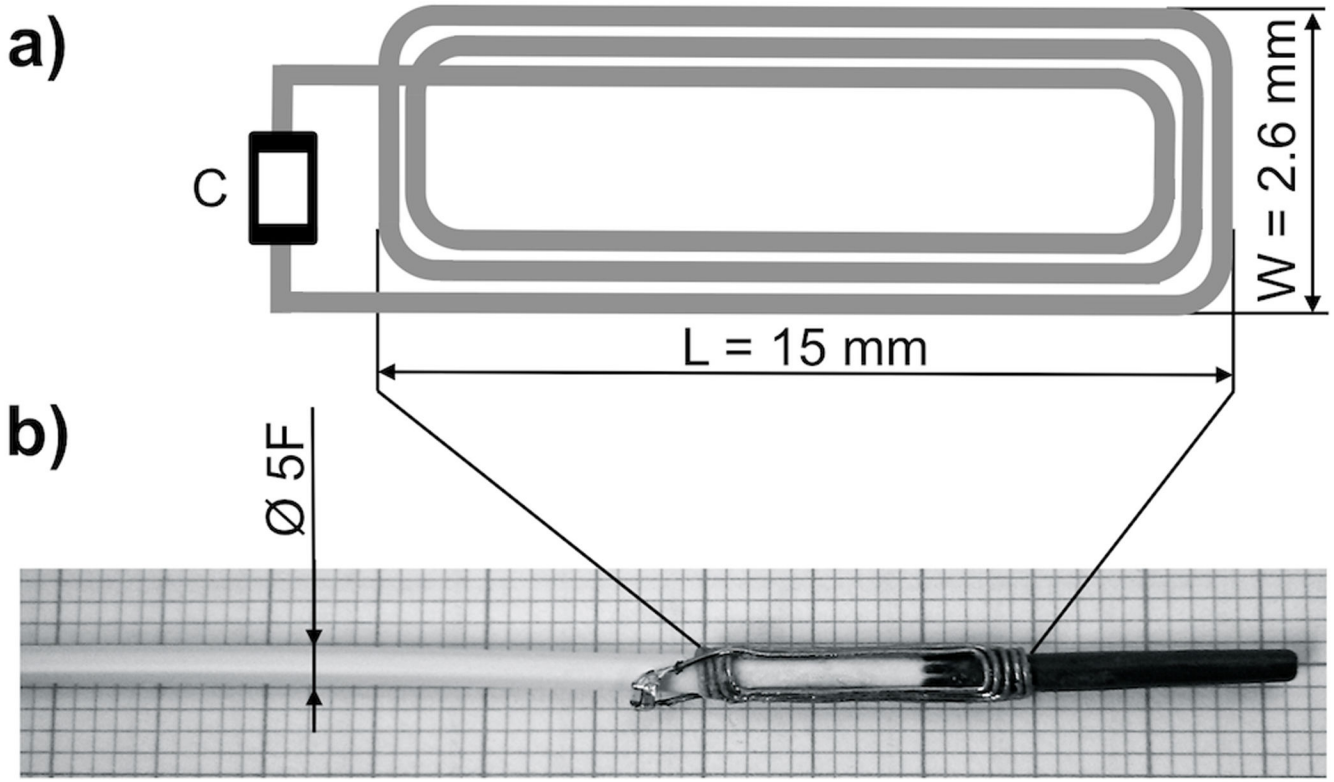

FIG. 2.

Schematic design of the wRC designed as a planar rectangular spiral coil with a non-magnetic SMD capacitor (C). The coil is wound with enamelled copper-wire, tuned to the Larmor frequency of the MRI system and connected to the capacitor. The wRC is then crimped around the catheters and coated with medical grade heat shrink tubing. A photographic image (b) shows the wRC on a 5-French straight catheter (without coating) and the enlarged schematic drawing (a) illustrates the coil design.

FIG. 3.

Balloon angioplasty performed in a clinical whole body 1.5T MRI scanner (Signa HDx, GE Healthcare, Waukesha, WI, USA). The catheter was manipulated in front of the bore while the catheter was tracked and the scan plane updated and displayed accordingly. The pictures were taken from three wireless IP cameras (M1031W, Axis, Lund, Sweden) that were installed in the scan room. All three images were acquired at the same point in time on (a) the left camera, (b) the right camera and (c) the camera behind the bore with a 10× zoom lens. The interventional radiologist was able to monitor the procedure on a 40” in-room monitor NEC (Multeos 401, NEC Corporation, Tokyo, Japan) and adjust the scan acquisition on demand or with a wireless input device as described elsewhere (47).

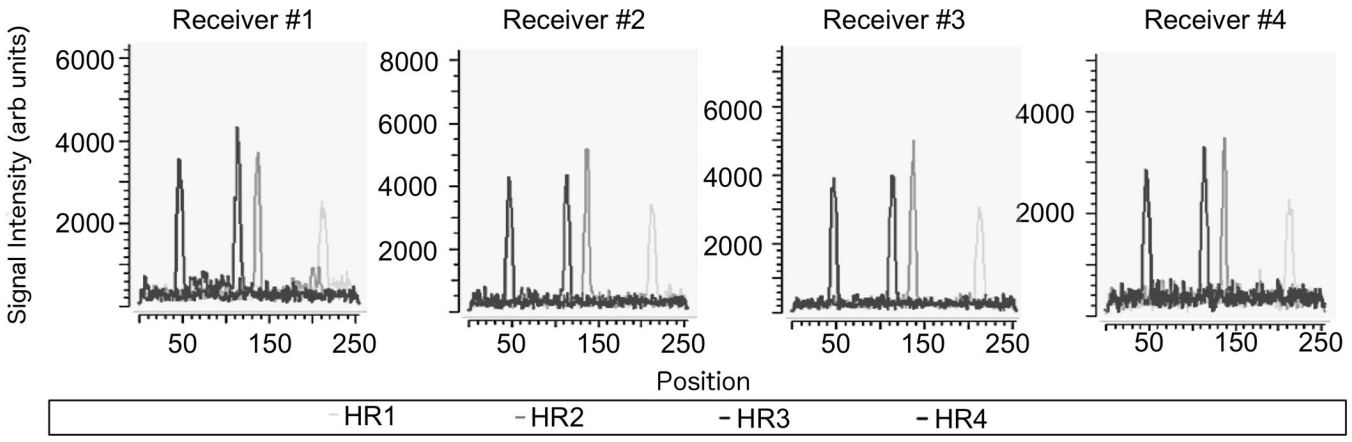

FIG. 4.

Signal plots post fast Fourier transform (FFT) while each of the four different coil channels was receiving MR-tracking signals during a tracking cycle with phase-field dithering (N=3). The catheter coil peaks in the four Hadamard modulated readouts (HR) can be distinguished from the background noise for each coil element. The catheter position was computed from the coil element with the highest peak-to-noise ratio (PNR) averaged over the 4 HR. The pulse sequence then emitted a new geometry update. The PNR was found to exceed a value of 15 along all readout directions (data not shown) during catheter navigation in the perfused phantom. Note that this figure exemplarily shows the coil plots for a specific phase field dithering direction (maximum PNR). The other phase field-dithering directions affected the amplitude of each peak (and therefore PNR) but not its position.

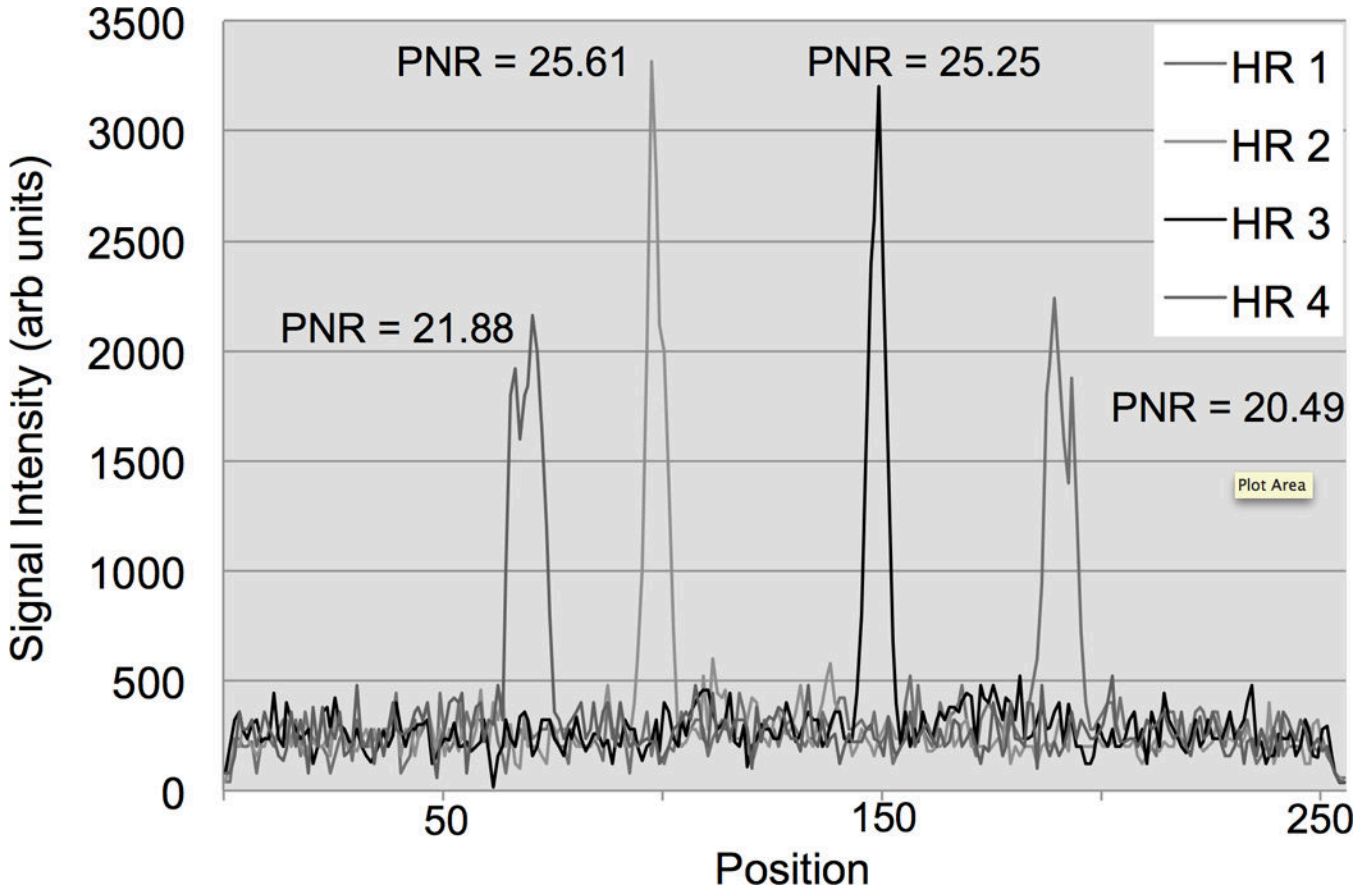

FIG. 5.

MR-tracking signals post fast Fourier transformation (FFT) from a phase-field dithering cycle (N=3) using the 5-French straight catheter in the perfused arterial phantom. The plot displays the coil element with the highest peak-to-noise ratio (PNR) averaged over the 4 Hadamard modulated readouts (HR). The catheter coil peaks / locations in the four HR can be distinguished from the background noise (isotropic tracking resolution = 1.8 mm).

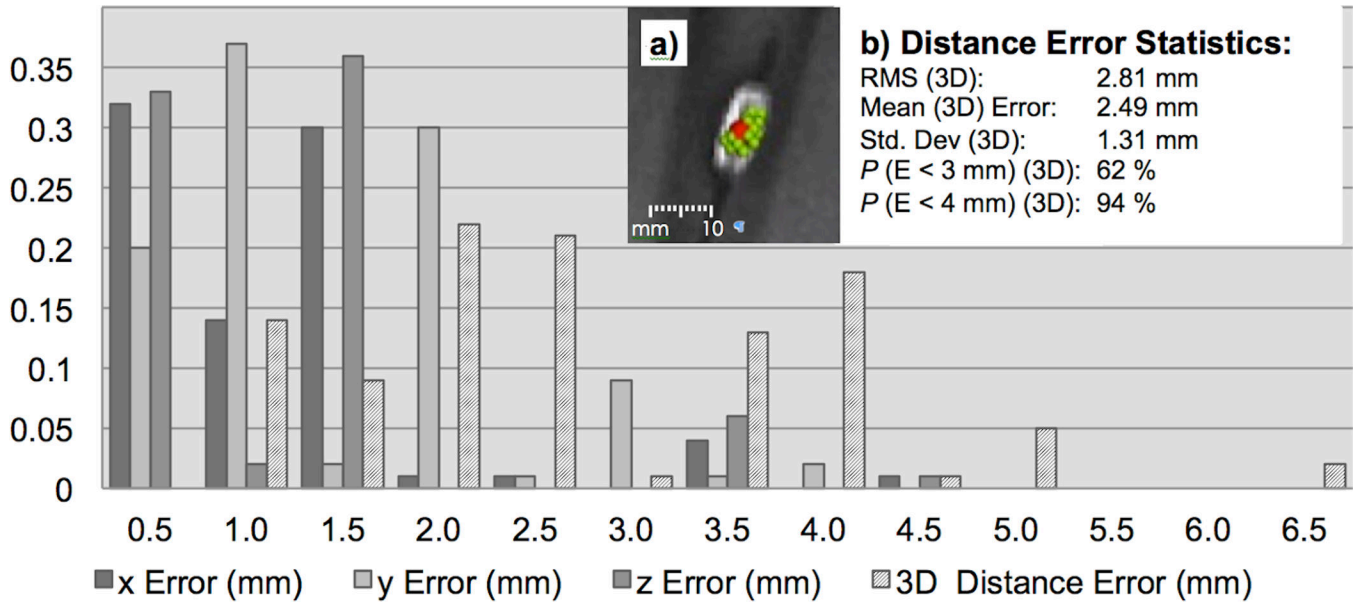

FIG. 6.

Distance errors (mm) represented as a frequency histogram - The error (E) represents the distance between the tracking position and the centre of gravity of the wRC on the catheter (Xc,Yc,Zc). The centre of gravity is indicated as red sphere in (a). The green points in (a) show the tracking point history (n = 1000) for one fixed catheter position in the vessel phantom. The statistical summary for the distance error is displayed in (b). Note that the distance error is calculated from the centre of gravity of the wRC and not the red sphere that is displayed in (a). As demonstrated in the graph, all points were found to be inside the area with enhanced signal intensity caused by the wRC on the catheter tip.

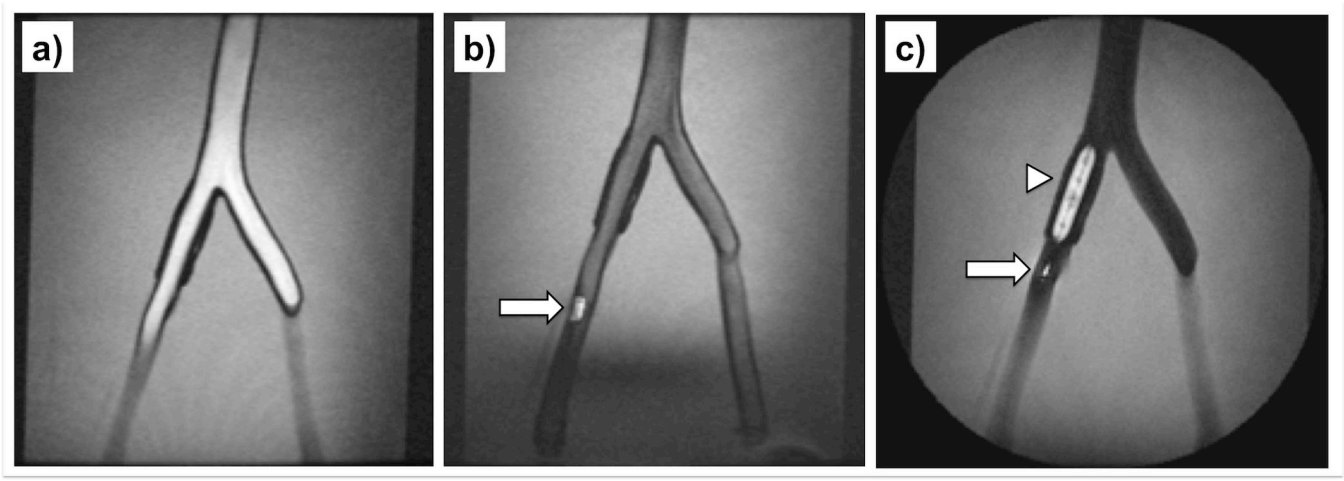

FIG. 7.

MRI-guided balloon angioplasty of the right iliac artery in the perfused arterial phantom. The rt-MRI sequence received a tracking update from the tracking pulse sequence and the pulse sequence and parameters were switched on the fly over the user interface - bright blood imaging (a) with bSSFP (TE/TR = 2.5/5.0 ms, FA = 70°, FOV = 30 cm, Matrix 256×256, Slice thickness = 2.5 mm). The straight catheter (wRC is illustrated as arrow) was advanced (b) while the FA is reduced in the bSSFP to FA = 30°. The catheter was then exchanged with a balloon (wRC is illustrated as arrow) catheter and inflated (c) with a 1:100 Gadolinium doped solution and once the catheter was in position, a balloon inflation (arrowhead) was performed under FSPGR imaging (TE/TR = 2.8/7.0 ms, FA = 70°, FOV = 30 cm, Matrix 256×256, Slice thickness = 7 mm).

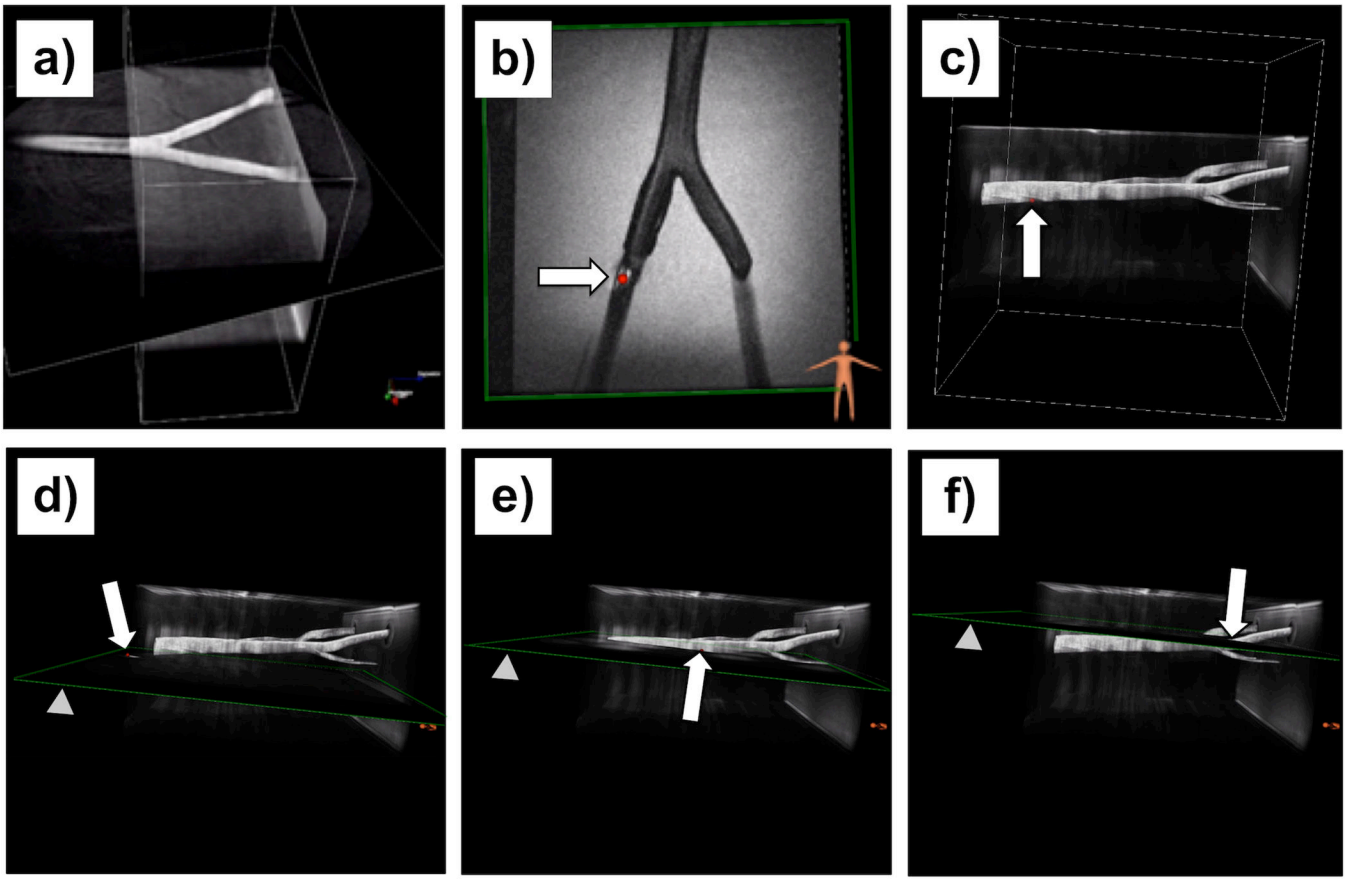

FIG. 8.

Wireless device tracking in the vascular phantom demonstrated in 2D and 3D. (a) A (2D) spGRE plane was fused to a previously acquired maximum intensity projection (MIP) of a non-contrast-enhanced MR angiogram while no device was present. Note the image, obtained with the spGRE (TE / TR = 3.5 / 20.4 ms, FA = 30°, FOV = 24 cm, 5 interleaves, Slice thickness = 8 mm) and a frame rate of 10 images per second, shows a black area right before the aortic bifurcation due to the present turbulence. (b) The catheter was inserted and the imaging plane (FSPGR, TE/TR = 2.8/7.0 ms, FA = 70°, FOV = 25 cm, Matrix 256×256, Slice thickness = 7 mm) was automatically re-aligned based on the tracking position of the wRC (arrow). Image (c) demonstrates the catheter position (sphere pointed out by arrow) rendered to the MRA roadmap. Images (d – f) show the same roadmap and a moving catheter while a 2D spGRE (same parameters as above) scan plane (arrowhead) is automatically realigned to the current catheter position (red sphere pointed out by arrow).

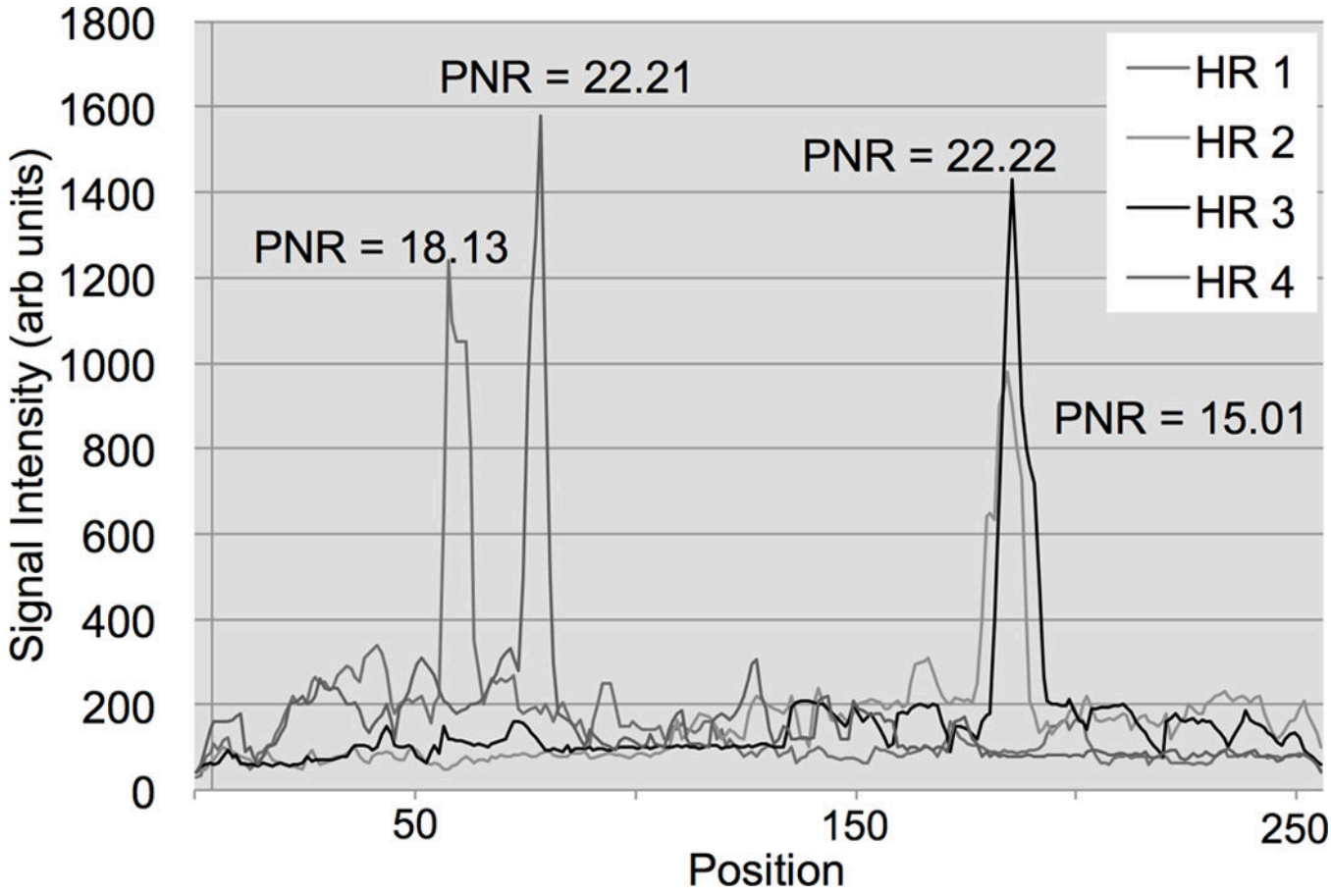

FIG. 9.

MR-tracking signals post fast Fourier transformation (FFT) from a phase-field dithering cycle (N=3) while the 5-French straight catheter was positioned in the femoral of a Thiel soft-embalmed human cadaver. The plot displays the coil element with the highest peak-to-noise ratio (PNR) averaged over the 4 Hadamard modulated readouts (HR). The catheter coil peaks / locations in the four HR can be distinguished from the background noise (isotropic tracking resolution = 1.8 mm). Note, smoothing of the curve and a FA of 1.5° were applied to improve the PNR for the tracking pulse sequence for the cadaver experiments.

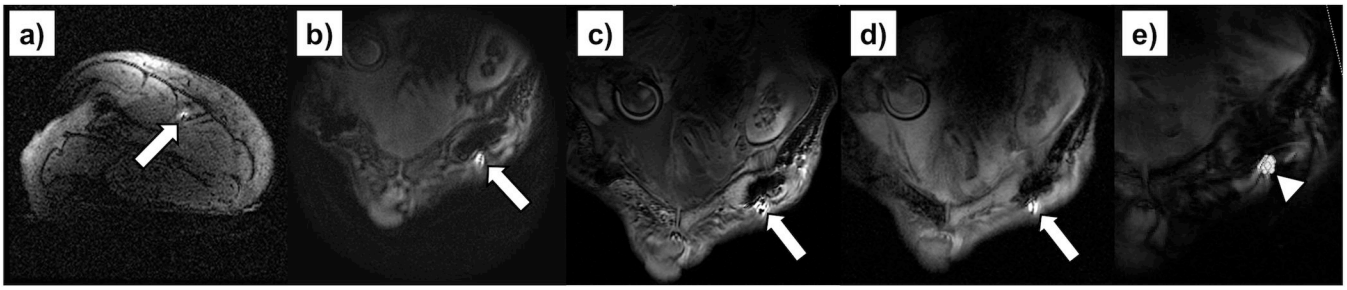

FIG. 10.

MRI-guided catheter navigation in the left femoral artery of a Thiel soft embalmed human cadaver. The arrow indicates the wRC that appears very bright compared to the background tissue. An axial FGRE (TE/TR = 5/11.8 ms, FA = 20°, FOV = 21 cm, Matrix 256×256, Slice thickness = 5 mm) localiser slice (a) that contains the wRC is displayed. The rt-MRI sequence received a tracking update from the tracking pulse sequence and the pulse sequence and parameters were switched on the fly with the user interface. Images obtained with (b) a FSPGR sequence (TE/TR = 2.8/7.0 ms, FA = 70°, FOV = 25 cm, Matrix 256×256, Slice thickness = 7 mm), (c) a bSSFP sequence (TE/TR = 2.5/5.0 ms, FA = 70°, FOV = 30 cm, Matrix 256×256, Slice thickness = 2.5 mm) and (d) a spGRE sequence (TE / TR = 3.5 / 20.4 ms, FA = 30°, FOV = 24 cm, 16 interleaves, slice thickness = 8 mm). On the right (e) the history of 1000 tracking points (arrowhead) for a fixed catheter position was overlaid on a magnitude image of the cadaver.